First UK field application and performance of microcapsule-based self-healing concrete

Abir Al-Tabbaa[a], Chrysoula Litina*[a], Petros Giannaros[a1], Antonios Kanellopoulos[a2] and Livia Souza[a]

[a]Department of Engineering, University of Cambridge, Trumpington Road, Cambridge CB2 1PZ, UK

*Corresponding authors:
Chrysoula Litina, cl519@cam.ac.uk, Department of Engineering, University of Cambridge, Trumpington Road, Cambridge CB2 1PZ, UK

Abstract

Maintaining the health and reliability of our infrastructure is of strategic importance. The current state of the UK infrastructure, and the associated huge costs of inspection, maintenance, repair and eventual replacement, is not sustainable and is no longer environmentally viable. The design of infrastructure, mainly concrete, remains traditional and poor material performance continues to be the main cause of deterioration and failure in our infrastructure systems. Biomimetic materials, that emulate natural biological systems in their ability to self-healing, provide an exciting and plausible solution. Embedding cementitious materials with in-built capabilities to sense and respond to their environmental triggers could potentially eliminate all external interventions and deliver a resilience infrastructure. The work presented in this paper forms part of a national initiative that has been developing biomimetic cementitious infrastructure materials which culminated in the first large-scale field trials of self-healing concrete in the UK testing four different but complementary technologies that were developed. This paper focuses on one self-healing technology, namely microcapsules, which contain a healing agent that is released on their rupture as a result of crack propagation. The paper will present details of the microcapsules used, their implementation in concrete and in the field trials and time-related, field and laboratory, assessment of the self-healing process. It also highlights challenges faced and improvements that are now on-going to produce the next generation of the microcapsule self-healing cementitious system.

Keywords

Self-healing, concrete, site trials, materials for life. microcapsules, applications, construction, materials, testing

[1] Present address: Klohn Crippen Berger, Vancouver, BC, V5M 4X6, Canada

[2] Present address: School of Engineering and Technology, University of Hertfordshire, College Lane Campus, Hatfield, AL10 9AB, UK

1 Introduction

1.1 Infrastructure and biomimetic materials

Infrastructure assets (e.g. bridges, tunnels, motorways, dams and embankment) are a nation's lifeline and are vital for societal and economic growth. The deteriorating state of the ageing UK infrastructure, and similarly around the world, is the result of decades of underinvestment. The UK recently committed to an investment of £500 Billion in infrastructure by 2020-2021 [1] in valiant efforts to save the nation's infrastructure assets. The majority of infrastructure assets are made out of cementitious composites, mainly concrete. Current figures show that half of the construction budget is spent on the repair and maintenance of mainly concrete infrastructure at around £40 Billion/year [2]. Concrete deterioration is the result of traditional civil engineering design practices that are still based on the assignment of appropriate partial material and action factors and providing redundancy to prevent failure. Material degradation is viewed as inevitable and mitigation necessitates expensive inspection, maintenance, repair and replacement regimes. Hence poor material performance continues to be the single main cause of deterioration and failure in our infrastructure systems. Moreover, the durability of repaired concrete structures continues to be major concern as after 5 years, 20% of all repairs fail, increasing to 55% after 10 years [3].

While the construction industry is the single largest consumer of resources and raw materials, and accounting for 6% of GDP, it remains the slowest sector to adopt and adapt to new technologies and advanced materials, due to its historic conservative approach to product design and delivery [4]. Construction materials have historically suffered from being perceived fundamentally as a cheap and straightforward commodity, where the application of often expensive cutting-edge material technologies is simply not justified. This view can no longer be sustained due to the huge volumes used and associated high carbon footprint as well as the extensive and expensive maintenance regimes that are needed to maintain our infrastructure assets. A new approach to material design through mimicking natural biological systems, in their ability to self-heal, has been adopted in some sectors, with commercial success, through the development of a new class of biomimetic materials. Biomimetic materials are advanced materials that can transform our infrastructure by embedding resilience within its components and systems so that rather than being defined by individual events, they can evolve and adapt over their life span. National and international government and industry road-mapping reports [4–7] have highlighted that advanced infrastructure materials, with specific reference to biomimetic attributes, will play an essential part in the future transition of infrastructure. This will provide a much higher level of confidence in the reliability of the performance of our infrastructure systems but will also require a complete paradigm shift across the design, procurement, construction and maintenance of our infrastructure.

In cementitious systems, while different forms of damage result from the wide range of environmental and mechanical actions, cracking is the most widely and commonly encountered. As a result self-healing of cracks in cementitious systems has been widely studied [8,9]. In this context, self-healing phenomena in cementitious systems are broadly classed into two categories: Autogenic and Autonomic (Fig. 1a-b). Autogenic self-healing refers to self-healing processes that are an intrinsic characteristic of the components of the matrix which are usually effective for small crack widths of ≤0.15mm and under water curing. Autonomic self-healing refers to actions that use components that do not naturally exist in the cementitious composite, i.e. 'engineered' additions that are usually employed to deal with larger crack sizes and under less favourable curing environments. Some autogenic and autonomic self-healing systems work in combination so that the autonomic system works to reduce the crack size to enable autogenic processes to complete the self-healing process. The work presented in this paper relates to the use of microcapsules for autonomic self-healing in cementitious systems.

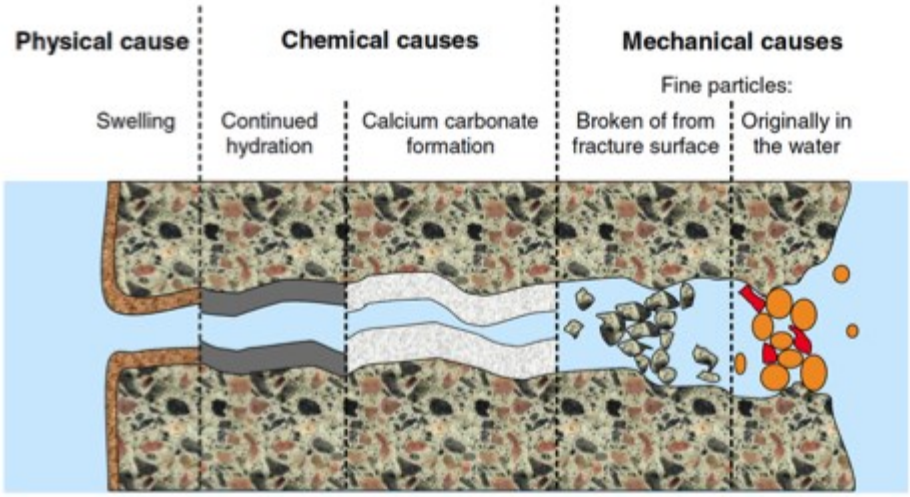

(a)

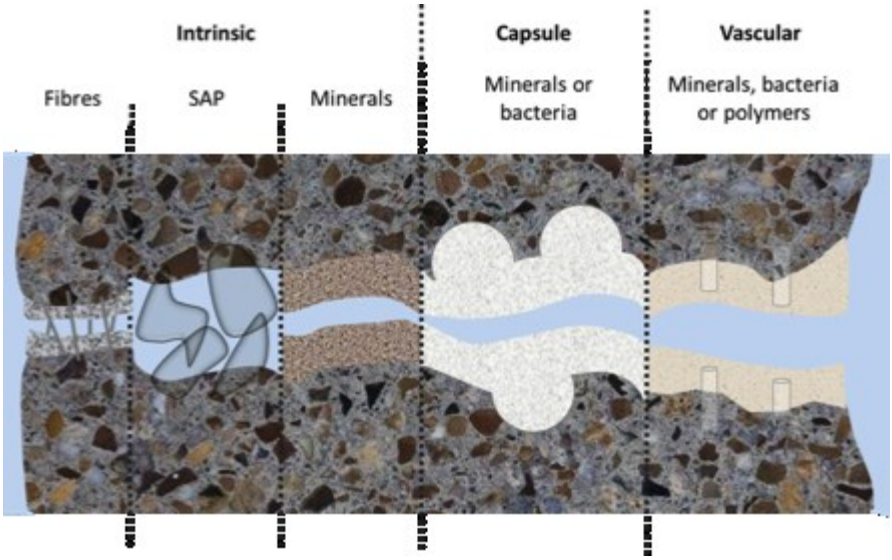

(b)

Figure 1 Self-healing mechanisms for cracks in cementitious systems (a) autogenic self-healing (Reproduced with permission, 2013 Springer [8]) and (b) autonomic self-healing (Reproduced with permission[10]).

1.2 Microcapsule-based systems for self-healing in cementitious systems

Microcapsules are micron-size particles consisting of a stable shell enveloping a cargo, which could be solid, liquid or gases, and serve a wide range of applications in different sectors. They are already in commercial use in construction materials for heat proofing, e.g. phase change materials, and air entraining agents, both incorporated directly into the building material mix composition [11]. Since White et al. [12] introduced the use of microencapsulation for self-healing of polymers in 2001, microencapsulated healing agents for autonomic self-healing has attracted much attention. Embedded microcapsules in materials imbue the ability of a localised response to damage upon rupture, and subsequent release and activation of the healing agent. The proof of concept for microcapsule-based healing in concrete was recently demonstrated [13,14]. The fundamental principle of autonomic self-healing via microencapsulation is that when cracks propagate in the cementitious matrix, they mechanically rupture the dispersed microcapsules and their content (cargo material) is released into the crack volume. Similar to encapsulation, the self-healing mechanism will rely on the nature of the cargo material; namely it may react with an activator (provided as a two-part system e.g. 2-part epoxy system), the cementitious matrix (including

hydration and carbonation products e.g. lime) or the environment (e.g. air, moisture for example cyanoacrylates) to form products that fill, seal or heal the crack (Fig. 2). Much of the published literature on microencapsulation-mediated healing has focused on cyanoacrylates or 2-part epoxy for their rapid hardening and high strength, hence quickly providing strength regain. However their high toxicity, high cost and short shelf-life prohibit their use commercially. Recent research has focused on the development of suitable microcapsules taking into consideration parameters affecting the bond strength and boundary conditions to enhance chemical compatibility with the cementitious matrix. Moreover healing agents that can deliver healing products of more compatible nature to the concrete matrix such as encapsulated bacterial spores and mineral cargos including colloidal silica and sodium silicate have recently been considered. A review of the various microcapsules systems can be found elsewhere [9].

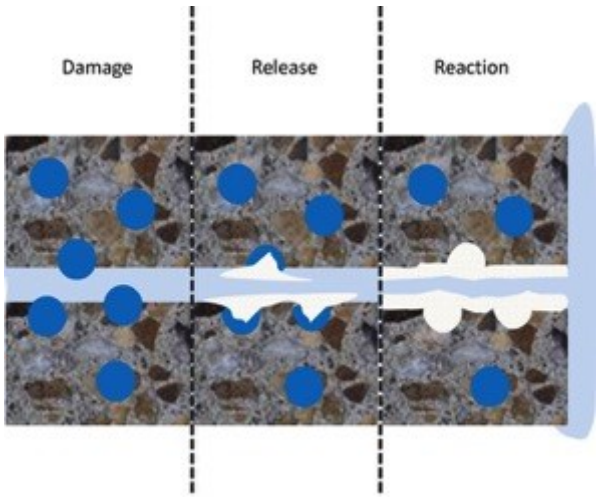

Figure 2 Schematic of microcapsule mediated self-healing in concrete [10]**.**

A number of experimental procedures have been developed and used to assess the self-healing efficiency in cementitious systems which include quantification of the mechanical recovery (e.g. compressive and flexural strength) using multiple cycles of static loading and reloading or non-destructive measurements as well as permeability measurements [15]. A review of the recent literature, relevant to self-healing microcapsules, shows changes in a variety of material properties when adding microcapsules into cementitious mixes; including workability, permeability, elasticity and strength, although the exact effect is highly dependent on the dosage, size, cargo and particular characteristics of the microcapsules [9] **.**

Previous work by the authors confirmed the potential of mineral microencapsulated cargos, in glass tubes, for use in self-healing cementitious materials, with a focus on sodium silicate [16,17] which is commonly used as a repair agent. Different polymeric microencapsulation systems for the sodium silicate were considered [10,18]. The most promising developments included the production of microcapsules with polymeric gelatin/gum Arabic shell, with switchable mechanical properties that ensured the required performance during the mixing and in response to a mechanical trigger [19]. The effect of these sodium silicate containing microcapsules was investigated on both the fresh (viscosity, setting time) and hardened properties (modulus of elasticity, compressive and flexural strengths) [19–21]. In these studies, work was also carried out on identifying the healing potential of these microcapsule-based systems under different cracking regimes and degrees of damage. While mineral healing agents do not provide the same level of mechanical strength recovery as its cyanoacrylate counterparts do, they were show to provide significant permeability reduction, hence providing efficient sealing and healing that will prevent ingress of aggressive chemicals and protect against corrosion.

1.3 Large-scale and field application of self-healing concrete

To date, most of the developments on autonomic self-healing cementitious systems have largely taken place in the laboratory. The first scale-up application of self-healing technologies in concrete was carried out in the 1990s by Dry at the University of Michigan simulated different damage scenarios for bridge elements and pavements in full scale and later field scale trials [22]. Reinforced concrete beams (0.15m x 0.15m x 1.8m) were constructed with embedded continuous brittle glass tubes in their tensile side. Three different healing agents were investigated including a two-part epoxy, cyanoacrylate and a silicon-based adhesive. The reinforced concrete beams were cracked to failure under three-point bending, allowed to recover and then retested to assess the potential for mechanical recovery. Although the reported results were inconsistent as to the performance of the healing technology, some strength regain was possible. Since then, other scale-up work of reinforced concrete samples with embedded glass tubes containing self-healing agents and subjected to cycles of loading and unloading was reported. Thao [23] considered a series of reinforced concrete elements embedded with glass tubes containing an isocyanate prepolymer fastened to their reinforcement bars. A concrete beam (125mm x 200mm x 2000m), concrete columns (200 x 800mm) and slabs (1000mm x 10000mm x 100mm) were investigated. When the beam was loaded under four-point bending, the embedded tubes showed breakage and subsequent release of the encapsulated agent. Columns were loaded to induce cracking and release of healing agents. Reloading of the column showed the formation of new cracks without any reopening of the previously healed cracks, due to complete recovery of the strength following self-healing. Subjected to impact-loading, the control slab showed a continuous loss in stiffness whilst the self-healing slab showed stiffness recovery up to 99%. Similarly Karaiskos et al [24] also added glass-encapsulated healing agents (polyurethane) into a 150mm x 250mm x 3000mm reinforced concrete beam. 350 glass tubes each 50mm in length were added 10mm from the base of the beam by attaching them to a plastic grid. Cracks were induced by loading the beam in four-point bending until the average measured crack width reached 0.25mm. Beams were then reloaded after a seven-week healing period and several non-destructive testing (NDT) methods were used to monitor healing of cracks. These included ultrasonic pulse velocity, piezoelectric transducers, acoustic emission and digital image correlation. Results were compared with a control beam without the glass tubes. No significant recovery in mechanical properties was observed for either beam although the use of a variety of NDT methods proved useful for monitoring crack formation, propagation and closure.

Transfer of developed self-healing technologies from larger laboratory-scale experiments to field-scale structures has been limited. In addition to overcoming practical challenges of up-scaling the healing technology, the in-situ application of any self-healing approach possesses unique challenges and obstacles. Field scale reinforced concrete applications of capsule-based self-healing concrete have been implemented [25,26]. Full scale reinforced concrete bridge decks (7m x 1.2m x 0.075m) were constructed, embedded with discrete glass fibres (100µm) containing a combination of sealant/adhesives. Brittle fibres placed close to the surface of the bridge deck targeted transverse shrinkage cracking. After one month, the fibres were seen to break releasing the sealant creating a controlled expansive joint. The efficiency of the healing mechanism under mechanical damage was also investigated. Load-induced cracks were generated using a pneumatic jack at mid-span causing the glass fibres to break and release the adhesive into the cracks. Subsequent reloading of the bridge deck was also conducted to test the efficiency of the adhesive in the regain of mechanical performance. Increased strength regain was demonstrated compared to a control deck with new cracks opening during reloading before the original cracks reopened. Re-release of repair adhesives in second and third loadings occurred in all of the decks containing repair adhesives showing good long-term survivability of the encapsulated healing agent. A few large scale field applications of bacteria-based self-healing concrete have also been realised [27,28]. Here, bacteria were added into the concrete mix that metabolise added calcium lactate to produce calcium carbonate. The first field application involved 3m-long concrete linings for an irrigation canal in Equador containing LWAs impregnated with alkaliphilic spore-forming bacteria [29]. After five months, the cast concrete

showed no sign of cracking or deterioration and therefore its healing performance could not be evaluated. Researchers at Delft University of Technology were first to implement self-healing concrete in a building[28]. A lifeguard station consisting of bacteria-based concrete has also been built [30]. However, no publication of results of how the building is performing to date could be obtained.

A national UK team, from the universities of Cambridge, Cardiff and Bath, has come together, through research council funding, to develop the first generation of self-healing cementitious systems in the UK to address cracks across many length scales [31–33]. This led to the development of a suit of complementary technologies namely microcapsules, calcite precipitation bacteria, shape memory polymer tendons and vascular networks (Fig 1b). These can be used in isolation or in combination depending on the nature and extent of the damage. Extensive system development and material testing was carried out in the laboratory. Collaboration with industry partners led to scaling up of the technologies and to the first UK full-scale field trials of the developed system in concrete retaining wall panels, on the Welsh Government A465 Heads of the Valleys Upgrade scheme project. Five concrete panels were cast- each being 1.8m tall, 1m wide and 150mm thick (shown in Fig. 3). Details of the design and execution of the field trials were presented elsewhere [34,35]. One of the panels contained the developed microcapsules and there was a control panel without any microcapsules with which a comparison was made. This paper focuses on the former. It presents details of the scaling up of the microcapsules and their use in the field trials and subsequent performance and monitoring.

Figure 3 Self-healing concrete wall panels constructed within the EPSRC and industry funded Materials for Life (M4L) project [35]**.**

2 Materials and Testing

2.1 Microcapsules and concrete mixes

The microcapsules used here were the result of industrial collaboration, which led to the design and production, using complex coaccervation, of gelatin/gum Arabic shell microcapsules containing sodium silicate (SS) as the cargo [19]. The sodium silicate was in an emulsion with mineral oil and emulsifier and formed ~42% of the cargo. The microcapsules (seen in Fig. 4a) had a mean diameter of 290µm with a standard deviation of ~120µm and were provided in a preserving solution (Fig. 4b). The microcapsules had switchable mechanical properties such that they initially had ductile 'rubbery' behaviour, which guaranteed their survivability during concrete mixing, and then became brittle, and easy to fracture, in the set concrete as water was removed from the shell [19]. Based on the results from related laboratory studies on the effect of the microcapsules on the fresh and hardened material properties and healing potential of mortars [21] and concrete [36], 8% microcapsule content by volume of cement (v_f) was selected for application in the field trials. This dosage was found to provide an optimum level of healing, showed high compatibility with the mortar matrix and had negligible effects on the workability, setting time and strength development.

The concrete mix composition is detailed in Table 1. The microcapsules were first washed with water and filtered from their preserving solution before being added, in their slurry form, directly into the ready-mix C40/50 concrete using a portable 120L Belle concrete mixer. The microcapsules were added at 8% by volume of the cement, corresponding to ~2.67% by weight of the cement and ~0.47% of the total concrete mix. A small quantity of water was used to wash out the microcapsules from the container and as a result the effective water-to-cement (w/c) ratio of the concrete mix increased from ~0.43 to ~0.45. A control panel was also cast without any microcapsules.

(a) (b)

Figure 4 The microcapsules used in the field trials; (a) the microcapsules under the microscope [19] **and (b) microcapsule slurry as delivered to site** [35]**.**

Table 1 Composition by % weight of the ready mix C40/50 concrete (supplied by Hanson UK) and the microcapsules used in the site trial.

Material	Quantity for field trials (kg/m³ unless noted otherwise)
Cement (CEM I)	415
10mm Limestone aggregates	944
Limestone fines (0-2mm)	396
Marine sand	393
Water	179 (w/c 0.43)
Admix: Plasticiser	0.35 L/100kg cement
Admix: Retarder	0.1 L/100kg cement
Microcapsules (slurry)	11.1

2.2 Crack initiation and monitoring

The wall panels were designed to crack 500mm from the base upon loading, which was facilitated by using 16mm diameter starter bars on the front face up to the designed crack location, before changing to the 10mm diameter mesh to create a weak section in the panel as seen in Fig. 5. Loading was applied using a hydraulic jack positioned 1.5m above the base of the panels, i.e. near the top of the wall, that was used to pull a threaded bar; thereby inducing a cantilever load. A wailing beam attached to the front of the panel allowed a distribution of load across the width of the wall. Full details of the design and construction of the walls is given elsewhere [35]. Panels were painted with a black-and-white speckle pattern for digital image correlation (DIC) analysis to monitor wall displacements and associated strains that arise during loading and unloading (Fig. 6).

Prior to loading, air permeability measurements at various locations around the wall face were taken as initial reference measurements using a field permeability tester [37], particularly in the region where cracking was expected to occur (Fig. 7). The permeability of the concrete cover (that between the steel reinforcement and external environment) must be sufficiently sound as an indicator of

good durability. Air permeability testing allows a non-destructive measurement of the quality of the concrete cover on site and involves applying a vacuum inside a cell placed on the concrete surface and then measuring the rate at which the pressure returns to the atmospheric value. The two-chamber vacuum cell is connected to a pressure regulator that balances the pressure in the inner (measuring) chamber and in the outer (guard-ring) chamber. Data was collected automatically by the display unit and the permeability coefficient (kT) and the depth of penetration (L) of the vacuum was calculated. The air permeability measurements are generally in good agreement with laboratory methods [37] and the testing equipment adheres to SN 505 252/1, Annex E.

Figure 5 Wall panel reinforcement design to ensure cracking at ~500mm from the base of the wall panel.

Figure 6 The microcapsule wall panel half painted with a black-and-white speckle pattern for DIC analysis

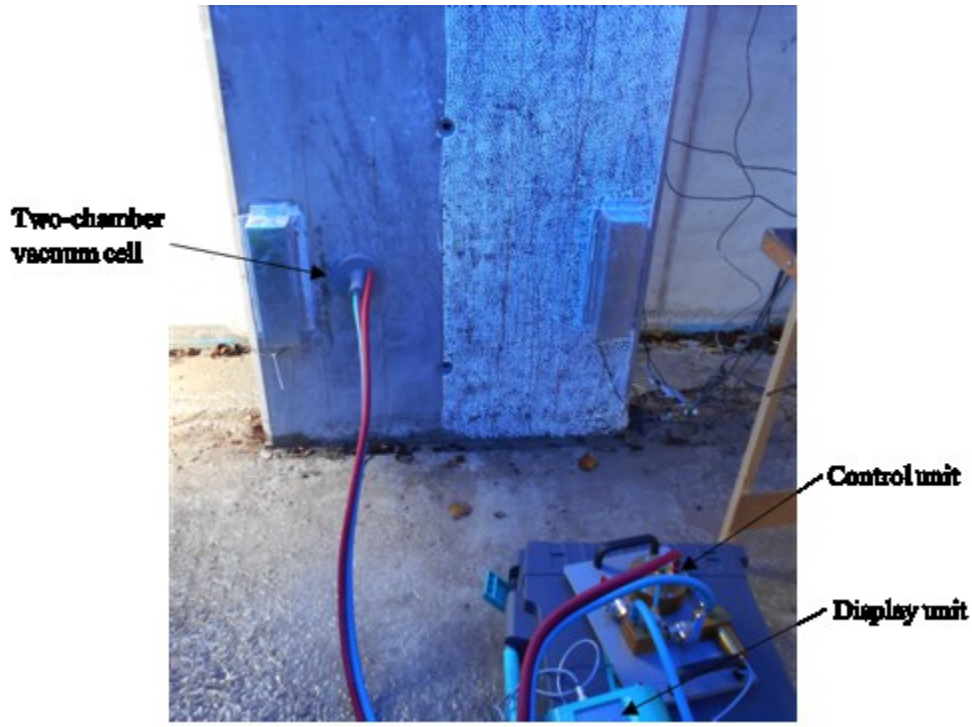

Figure 7 Air-permeability testing device obtaining measurements around the expected crack generation area.

A timeline of the field trials experimental programme is given in Fig. 8. The wall panels were initially loaded 5 weeks after their casting day and then reloaded after a 26-week healing period. Loading was applied until a noticeable crack appeared at the designed height and a large drop-off in load was

observed. After the healing and monitoring period, the walls were reloaded to the residual (drop-off) load. Four linear variable differential transformers (LVDTs) were used to measure lateral wall displacements. The LVDTs were located at the same height as the load application: two recording displacements of the wall panel and two recording displacements of the reaction wall. A mean of the lateral wall displacement was used when plotting load-displacement curves. A further two LVDTs were used to record crack opening by mounting them vertically on the front of the wall panel, ensuring that they span across the expected location of induced crack. Demountable mechanical strain gauge (DEMEC) pips were attached adjacent to the LVDTs to measure crack opening (Fig. 9). Once the panels were cracked, the load was kept constant and DEMEC measurements were taken. To complement the latter, microscope images were taken along the crack length spanning the panel width using a handheld digital microscope. After the acquisition of DEMEC measurements and microscope images, the load was gradually released from the wall panel. After complete unloading, DEMEC measurements and microscope images were taken once again, at the same exact points, to measure the residual crack width.

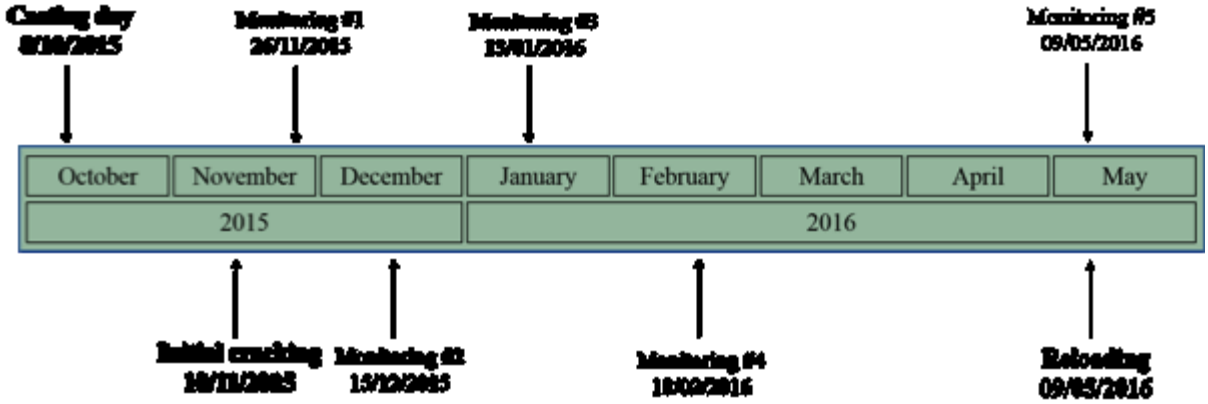

Figure 8 Timeline of wall panels testing and measurement collection dates

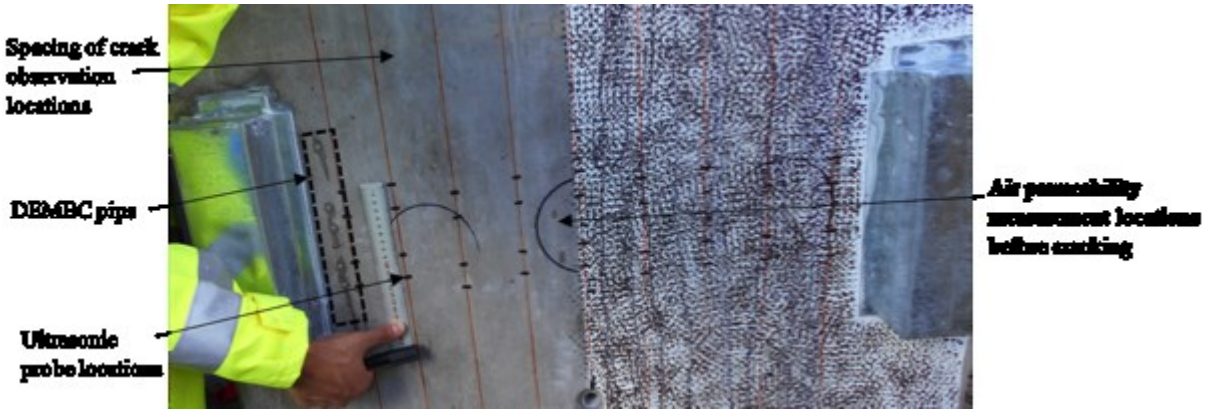

Figure 9 Location of DEMEC pips, ultrasonic probe measurement locations and air permeability measurement locations.

The DIC software measured displacements through the comparison of images to monitor movement in the speckle pattern. Photographs of the wall were taken at each kN load applied (or released) using two digital cameras and flash equipment set up on a tripod facing the wall panel (Fig. 10). The use of DIC allowed monitoring of crack initiation, coalescence and propagation. The covering of one-half of the wall face only in the speckle pattern offset any potential variations in obtained measurements due to the hydrophobic/water repellent nature of the paint. After initial cracking, a strip of thermal insulation foil roll was placed across the middle section the microcapsule wall to reduce its exposure to the environment. This was to examine the effect of sealing on the overall healing progress for both halves of the wall although the insulation was permanently removed after

Monitoring event #1. Weather data was collected from local weather stations in Tredgar and Usk between October 2015 and May 2016 including daily minimum air temperature, maximum air temperature and total rainfall.

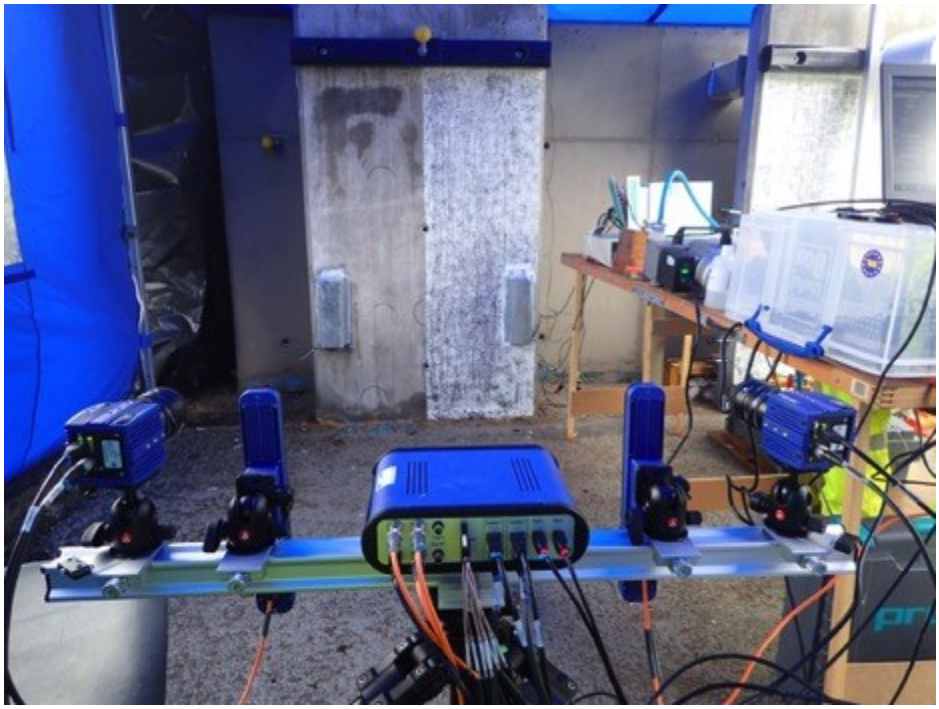

Figure 10 Digital Image Correlation camera and tripod set-up on the microcapsule wall.

Between initial cracking and reloading stages, various measurements were periodically taken from the wall panels to assess crack closure and monitor self-healing. Microscope images were taken from at least five observation locations along the crack length. Using this data, interpolation of crack width along the crack length was carried out allowing a visual representation of crack width across the wall panel throughout the healing period. Crack width healing values were also calculated in order to quantify crack closure. The crack width healing percentage compares measured crack width values with the initial crack opening at that point following cracking and load-release. Crack width healing (*CWH*) was calculated as shown in Equation 1:

$$CWH = \frac{w_i - w_h}{w_i} \times 100\% \qquad \text{(Eq. 1)}$$

where w_i is the initial crack width and w_h is the healed crack width.

Visual observations on the specimen surface only provide an indication of the extent of self-healing occurring at the crack mouth and do not provide insight into the healing processes that take place deeper into the crack. Therefore, non-destructive techniques such as the use of ultrasonic wave transmission and air permeability were used to provide information about internal densification and self-healing. An ultrasonic pulse velocity test instrument complying with European standard EN12504-4 and BS1881:Part 203 was used to measure the crack depth at each of the crack observation locations during the monitoring events. The ultrasonic probes were placed on the concrete surface adjacent to the crack and ultrasonic couplant was used between the surfaces to facilitate transmission. Water-saturation of the walls hindered both the ultrasonic and air permeability measurements throughout the monitoring period. Subsequently, only three monitoring events were possible for the former; namely after cracking, at 2 weeks and at 26 weeks (monitoring #1 and #5 respectively) whereas only two for the latter; after cracking and at 26 weeks (monitoring

#5). This was due to the consistently high levels of rainfall in the area particularly over the wet winter months.

2.3 Microstructural analysis

Following the re-loading of the wall panels, hence at 6 months, material was extracted from the crack surface after load removal. A multi-tool fitted with a grout removal attachment was used to carve our pieces of materials extract and also powder that was later passed through a 40µm sieve for laboratory investigations of the microstructure to quantify the products that formed in the cracks. Tests employed include scanning electron microscopy (SEM), X-ray Diffraction (XRD), thermogravimetric analysis (TGA) and differential thermogravimetric analysis (DTG). In addition, cores 100 mm in diameter and 200 mm high were also cored from the microcapsule wall and tested in a CT scanner to observe the homogeneity of the distribution of the microcapsules within the concrete and how intact they are.

3 Results and Discussion

3.1 Characteristic strength and mechanical loading

The characteristic cube strength obtained of the concrete mixes tested at 28 days without and with microcapsules were 59.3MPa ± 0.85 and 42.2MPa ± 3.8 respectively. Although previous lab work [36] had indicated that the addition of microcapsules would have a minimal effect on the strength of the concrete the observed values suggested a strong effect on strength development. It was stipulated that the great variation and discrepancy in results for cube strength for the site mixes is the result of significantly deteriorated workability and honeycombing. The reason for this being the double handling of the concrete to enable the microcapsules to be added to the mix as well as inadequate hand compaction of the cube specimen as a consequence of the casting sequence adopted on site.

The load-displacement relationship for both panels for initial loading and reloading seen in Fig. 12 confirm that the strength of the panel as not compromised by the addition of the microcapsules. This figure shows that both the initial peak loads obtained, 23.9kN and 21.9kN for the control and microcapsule panels respectively, and the residual loads, 17.4kN and 16.2kN respectively, suggest a smaller decrease (~8%) due to the presence of the microcapsules. Similarly, the concrete stiffness values were also seen to only decrease by ~8% from 7.8kN/mm in the control panel to 7.1kN/mm in the microcapsule panel. These results are in better agreement with the cylindrical compressive strength results for microcapsule-loaded concrete samples cast and tested in the laboratory (~9%) [36] as well as previous laboratory observations for mortars [21].

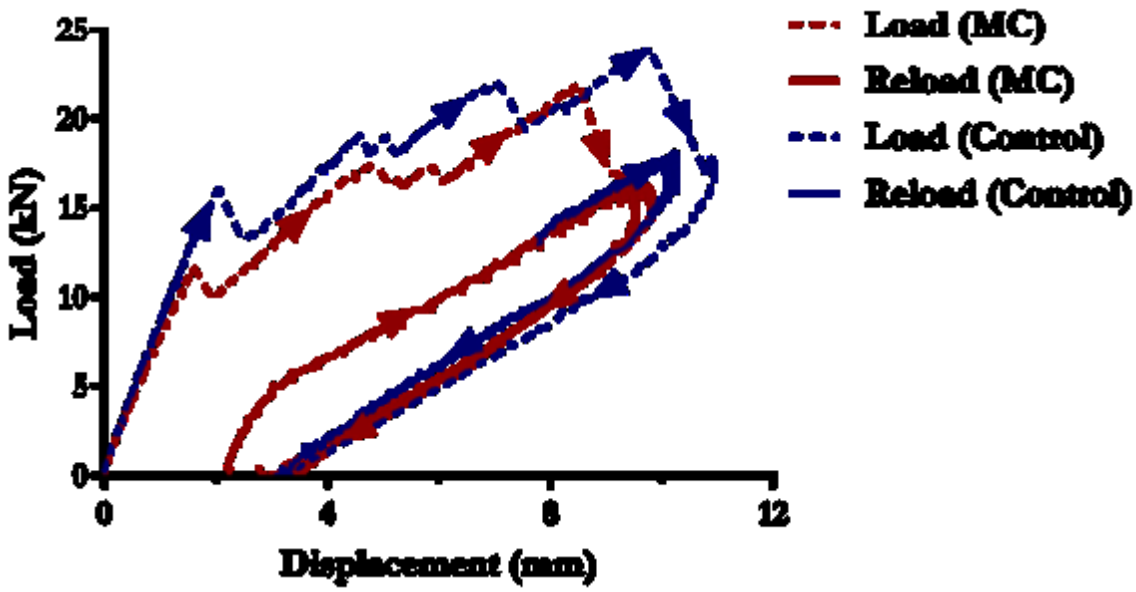

Figure 11 Initial and reload load-displacement curves for the microcapsule and Control wall panels.

Several microcracks were formed during loading, evident from the various drops in the load-displacement curves (Fig. 12a and 13a). The first crack was noticed at 16.1kN (~72% of maximum load) and 11.6kN (~55% of maximum load) in the control and microcapsule walls respectively. This microcracking was also clearly visualised in the DIC images showing vertical strain E_{yy} since loading induced tensile stresses normal to the plane of the crack (i.e. mode I crack separation). In the microcapsule panel, a microcrack formed at ~280-300 mm from the base before a second microcrack formed below this at between 30-100mm (Fig. 12b). In comparison, for the control panel, a microcrack first formed closer to the base at 50-100mm and then a second between 200-250mm (Fig. 13b). Despite those differences, two significant microcracks were formed in both walls between the designed crack location and the wall's joint with the base slab. The third crack was then generated at the designed location 500mm from the base, resulting in failure of the wall. Due to technical logging issues, the initial reload curve for the control panel was not obtained.

The DIC results show that during reloading it was the main crack that first re-opened before the opening of the other two microcracks occurred in both the microcapsule (Fig. 12b) and control wall (Fig. 13b), confirming that low strength regain is possible by autogenic healing or mineral based-autonomic healing. This is in agreement with previous unconfined compressive strength (UCS) and flexural laboratory tests on the microcapsule-based concrete system [36] where an addition of 8% microcapsules achieved 10% more strength than the control and an absolute strength recovery of 25% over the monitored period.

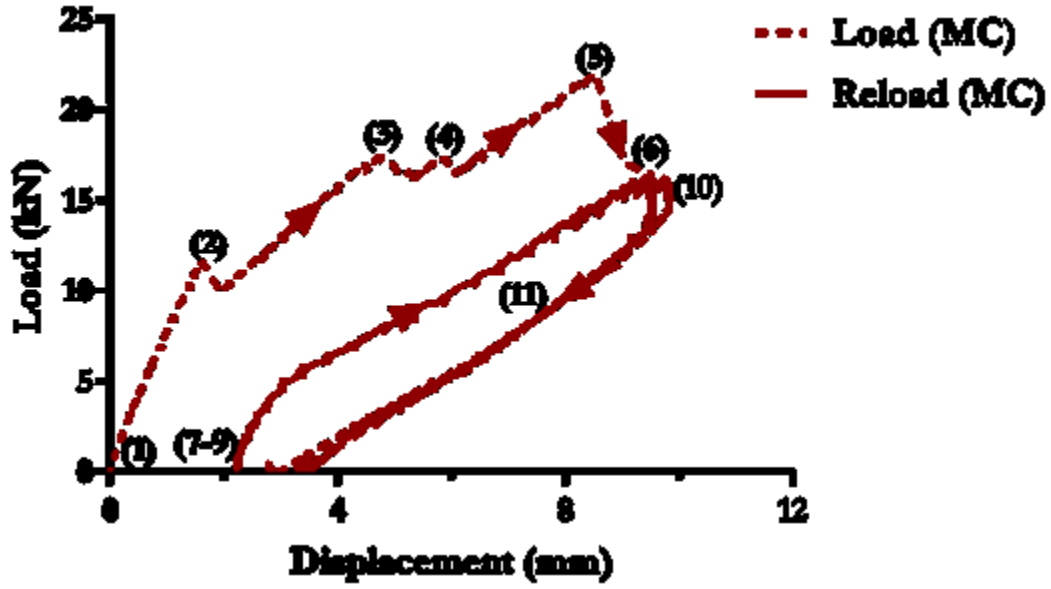

(a)

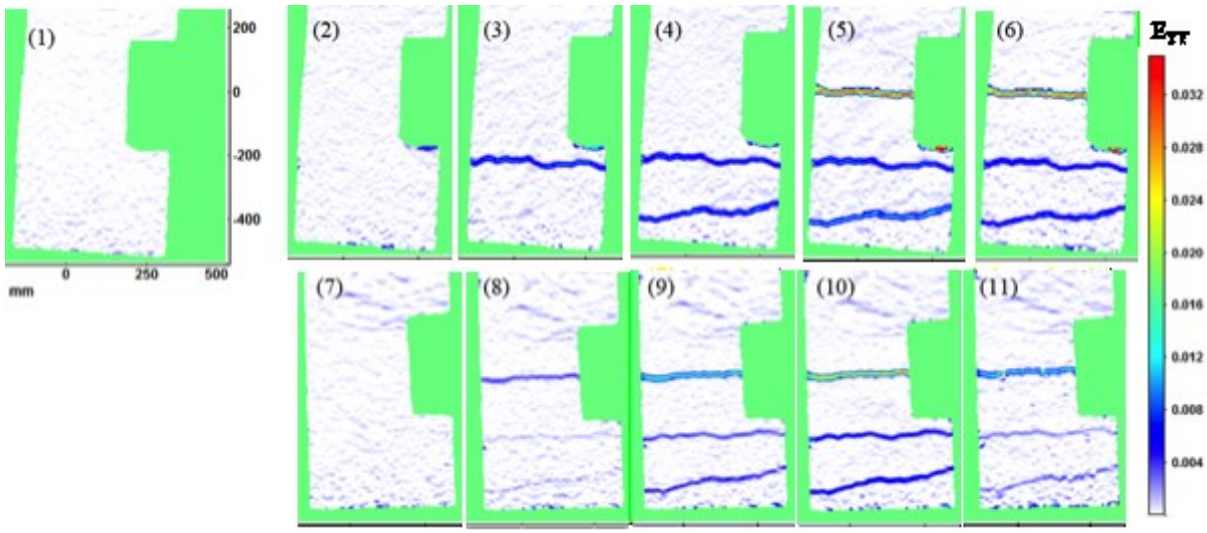

(b)

Figure 12 (a) Loading and reloading of the microcapsule wall and (b) corresponding DIC images.

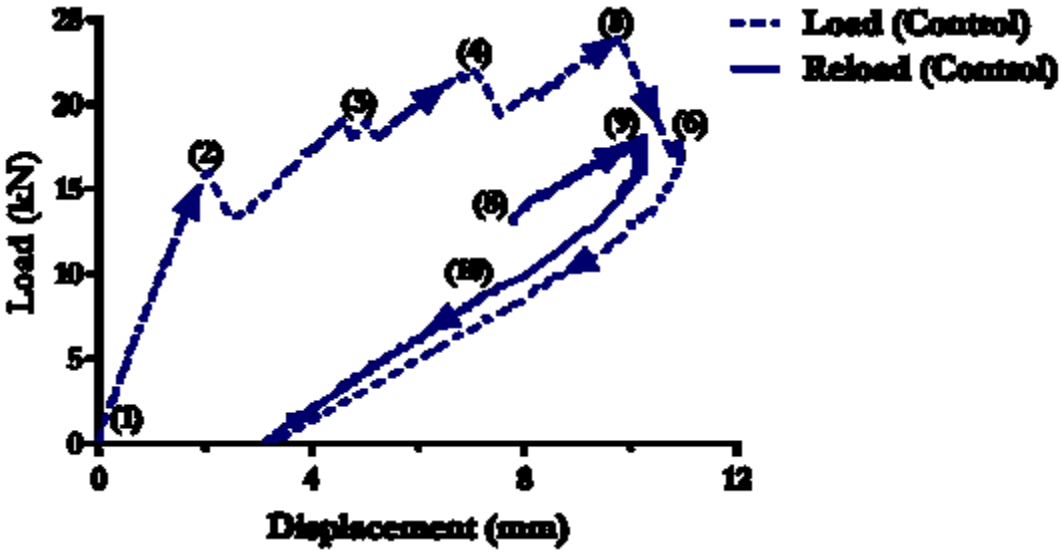

(a)

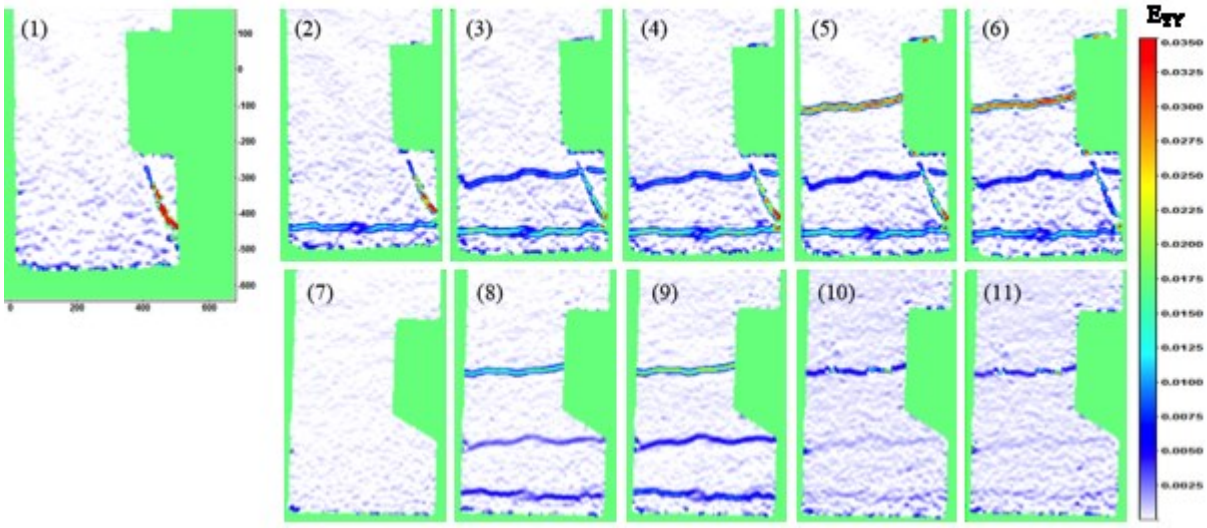

(b)

Figure 13 (a) Loading and reloading of control wall and (b) corresponding DIC images.

3.2 Microscopic crack healing

Following initial cracking and subsequent load release, residual crack width measurements were recorded from optical microscope images showing initial average crack widths of 165µm and 115µm in the control and microcapsule panels respectively, consistent with the lower load reached in the latter. The DEMEC and LVDT crack opening measurements results were comparable with those measured from the microscope images. The progress of healing was monitored throughout the 6-month testing period through microscope imaging of the crack width. During this monitoring period, no reduction in DEMEC and LVDT measurements was observed indicating that any reduction in crack width obtained is not from mechanical re-joining of the crack faces but rather due to the expected healing mechanism of depositions, filling and sealing within the crack.

Interpolation of crack width measurements on different locations along the crack length (shown in Fig. 14a) can be seen in Fig. 14b in which the colour-bar indicates the level of crack closure achieved. Similar crack width healing characterisics are seen in both panels with less healing observed on the right-hand side of wall panel due to the paint required for the DIC speckle pattern. The paint has a waterproof characteristic and therefore water runs off the surface rather than permeating into the

crack and contibuting to clogging of the crack mouth. Accelerated average crack healing along the main crack location, of 49% and 63% was evident as early as monitoring events #1 (14 days) and #2 (28 days) for the MC panel compared to 14% and 36% respectively, observed in the Control panel. These results not only confirmed preliminary investigation for mortars specimen [21] but also were in good agreement with microscopic crack width healing reported in laboratory concrete samples prepared with equivalent microcapsule content. The average crack width healing for cube, cylinder and prism concrete specimens after a 28-day water-immersed healing period was established in laboratory conditions prior to the field trials. There, microcapsule-containing samples showed superior crack closure- reaching ~50%, compared to the control samples with an average of less than 23% [36]. The large variations in areal healing observed in the control laboratory samples were also consistent with those observed for the Control panel on site.

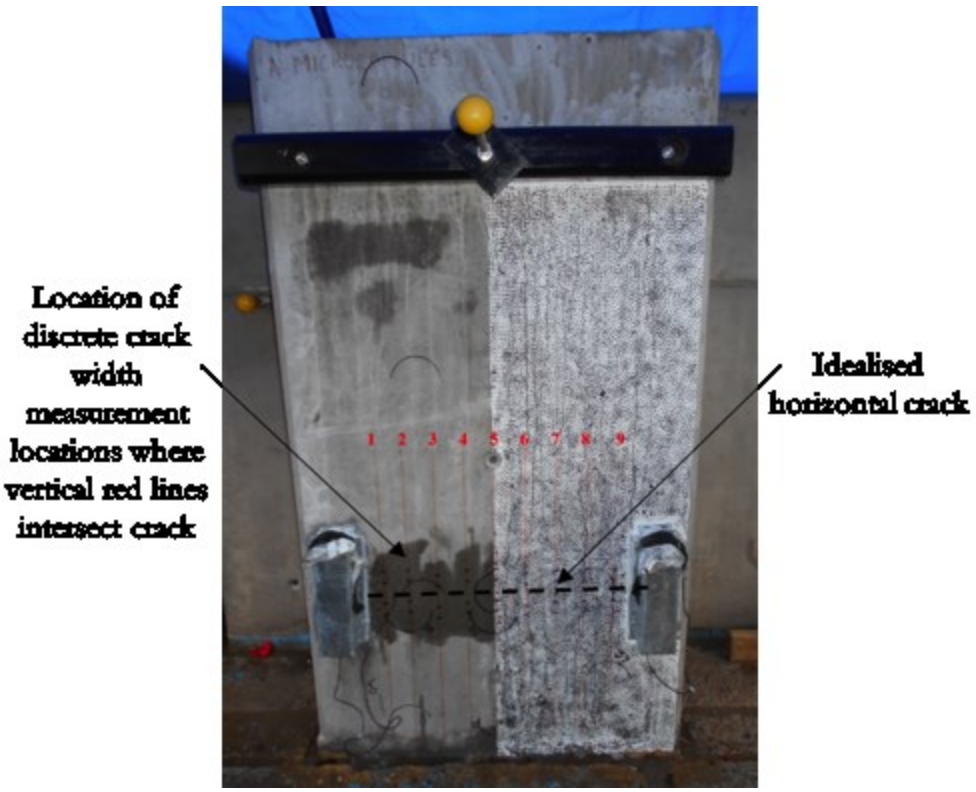

(a)

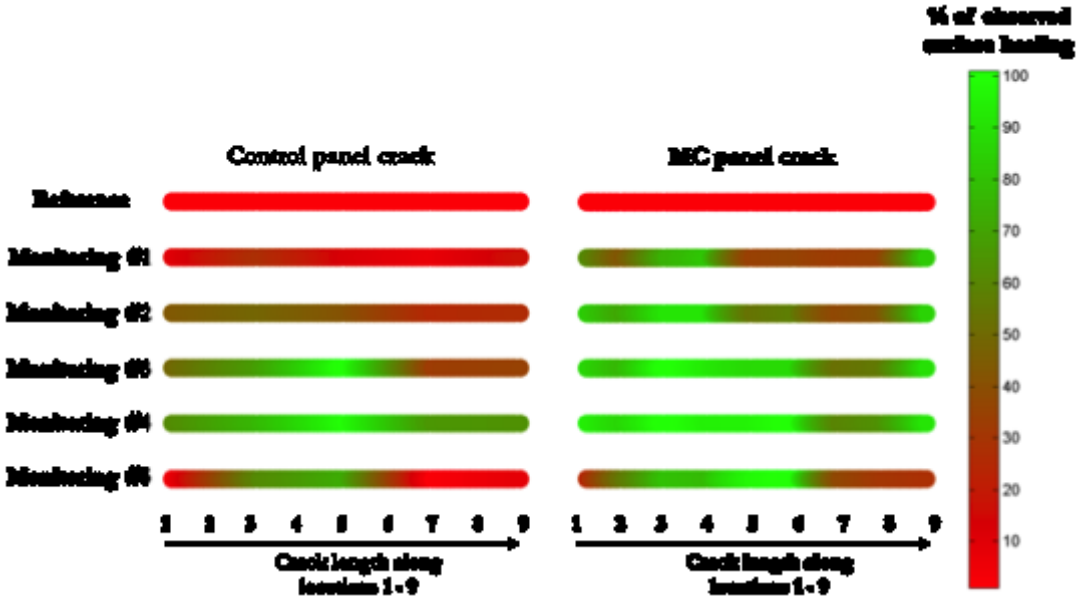

(b)

Figure 14 Monitoring crack width healing in panels: (a) microcapsules wall panel showing the locations (numbered 1-9) at which discrete crack width measurements were taken and (b) continuous crack width healing percentage plots for both panels.

Although the observed overall healing was within the expected range with final observed healing of 54% and 27% for microcapsule and control wall respectively, a temporal variation of the healing progression between monitoring events was observed in both panels. There is a clear increase in crack opening between monitoring event #4 and #5 for both panels although this is less prominent for the microcapsule wall. Thermal expansion and contraction due to changes in atmospheric temperature contributed to the change in crack width measurements. The mean crack width obtained over the monitoring period can be seen in Fig. 15a along with the daily average air tempreature obtained from local weather stations. Crack width measurements are normalised with respect to the width obtained following load removal (i.e. residual crack widths). A trend is clearly observed between the daily average air temperature and the normalised crack width in both the microcapsule and control panels. Crack width measurements constantly reduced during the first four monitoring events (between November 2015 and February 2016). However, the normalised crack width increased for the final monitoring event before reloading of the panels in May 2016 although the measured width is still less than the residual crack width measured upon initial loading of both panels. This indicates that variations in measured crack width cannot be solely due to thermal expansion and contraction but also due to self-healing contributions.

The crack in the microcapsule wall shows consistently greater closure than in the control wall throughout the monitoring period. In particular, the initial crack closure (indicated by the negative slope between the first and second measurements) is higher for the microcapsule panel. This indicates that the autonomic self-healing reactions have begun within the first two weeks after cracking. Studies that have explored the efficacy of sodium silicate as a healing agent have observed mechanical binding of sodium silicate with hardened cement paste [16,38] even within 48 hours [39]. It is no surprise therefore, that the autonomic self-healing benefit is realised within the first two weeks of cracking. Since temperatures did fall below 0°C in January and February, freeze-thaw damage may also have contributed to the observed behaviour. Free water that freezes within the concrete pores expands and exerts internal stresses to the material. These stresses may drive open pre-existing microcracks (thereby increasing the observe crack width) or may create new cracks in the material. Cycles of freeze-thaw can cause progressive and cumulative damage.

Observations of daily rainfall totals also suggest the contribution of rainwater to the healing process. Fig 15b shows the average normalised crack width along with daily rainfall totals. The greatest amount of rainfall is observed during the first three months after initial cracking; namely in December, January and February. Water is necessary for the reaction of the released sodium silicate with the hardened cement matrix. Furthermore, the presence of water is one of the most important criteria for successful autogenic self-healing [40,41]. The temporary addition of insulation to the micocapsule panel in the first two weeks of monitoring did not appear to have affected the obtained results. Theoretically, less self-healing is expected in the locations that were covered due to water deprivation in the cracks limiting both autogenic and autonomic self-healing processes. However, in this wet environment, the insulation tape was inadequate to provide protection from rainwater and the concrete quickly saturated under rainy conditions.

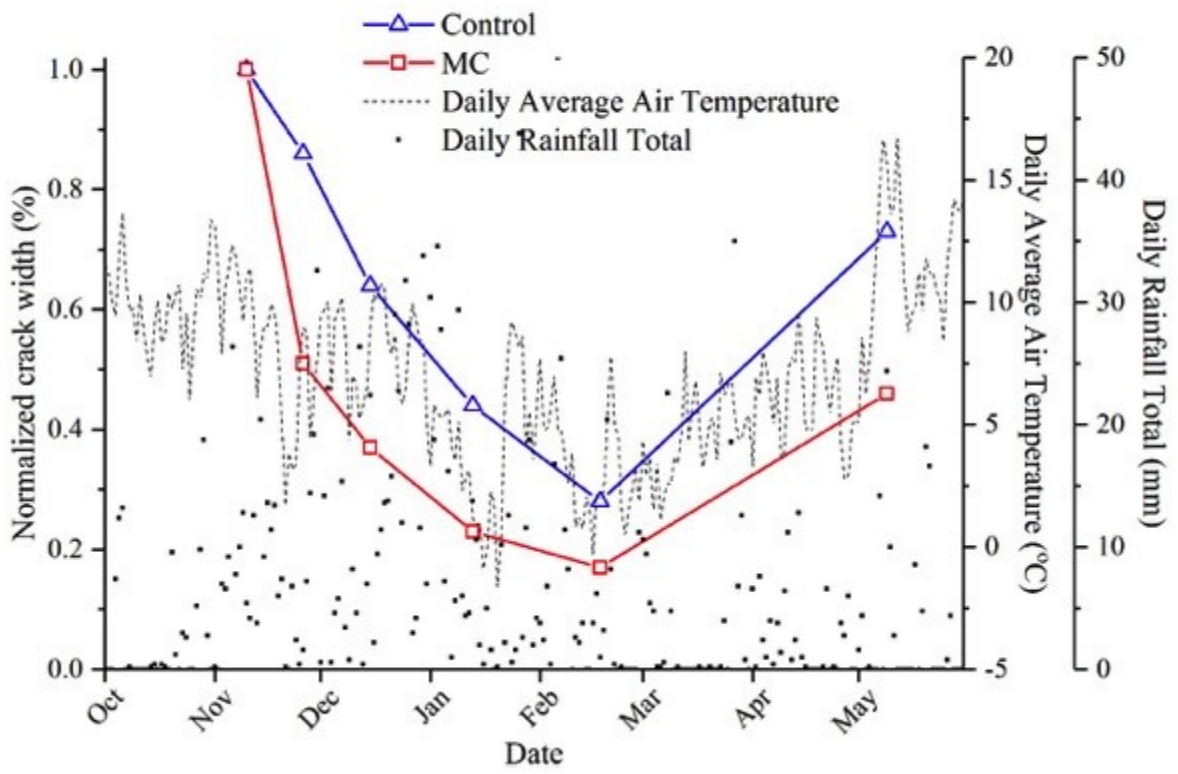

480

481 **Figure 15 Monitoring crack width healing in panels: (a) microcapsules wall panel showing the**
482 **locations (numbered 1-9) at which discrete crack width measurements were taken and (b)**
483 **continuous crack width healing percentage plots for both panels.**

484

485 ## 3.3 Crack depth and permeability

486 The crack depth measurements taken with the ultrasonic device on site are presented in Fig.
487 16. Only three monitoring events were possible; after cracking, after 2 weeks and after 26 weeks
488 (monitoring #1 and #5 respectively) due to a number of challenges faced with the testing on site,
489 since measurements were unreliable when the surface of the concrete was wet. In addition, the
490 uneven wall surface made the use of probes quite problematic. The average crack depth reduced by
491 ~8% and ~39% after 2 weeks (#1) and ~20% and ~58% after 26 weeks of healing (#5), in the control
492 and microcapsule walls respectively. Interestingly, the observed relative improvement by the
493 addition of microcapsules is higher compared to laboratory measurements (~28%) on concrete
494 samples produced with the same dosage of microcapsules.

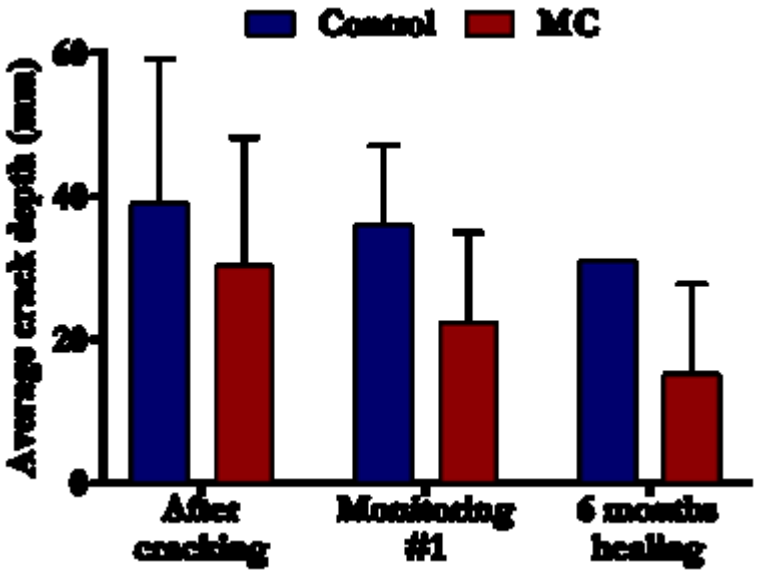

Figure 16 Average ultrasonic crack depth measurements after cracking, after 2 weeks and after a 6-month healing period.

The coefficient of air permeability values measured at three periods are shown in Fig. 17a, showing very similar values of ~10^{-19}kT for both walls before cracking suggesting that the microcapsules did not significantly alter the initial porosity of the concrete. This value is typical for concrete of very low permeability [42]. After cracking, the air permeability of the microcapsule wall was noticeably greater than the control wall by ~2 orders of magnitude. Since the microcapsule wall failed at ~8% lower load than the control panel and hence slightly weaker, it is possible that this had induced a greater content of internal microscale damage and cracking. It should be noted here, that it was not possible to obtain air permeability measurements after cracking from all of the same locations prior to cracking. When placing the device in locations directly over the induced crack, the device was unable to create a vacuum and therefore obtain a reasonable measurement. Since the crack passed through the initial measurement locations, new locations adjacent to previous measurement locations were chosen (Fig. 17b). At monitoring stage #5 (6 months of healing), the permeability of the control panel reduced only slightly, while that for the microcapsule wall recovered significantly, by >2.5 orders of magnitude, to ~10^{-18} kT. The permeability of the microcapsule wall was half an order of magnitude less than the control wall and was consistent with trends observed in the laboratory using sorptivity tests. The average sorptivity coefficients calculated across control and microcapsule-containing concrete samples after a 28-day healing period show that the rate of water absorption by microcapsule loaded samples is generally lower than that of the control [36]. Nonetheless the permeability of both walls remained greater than the permeability prior to cracking indicating only partial self-healing at that stage.

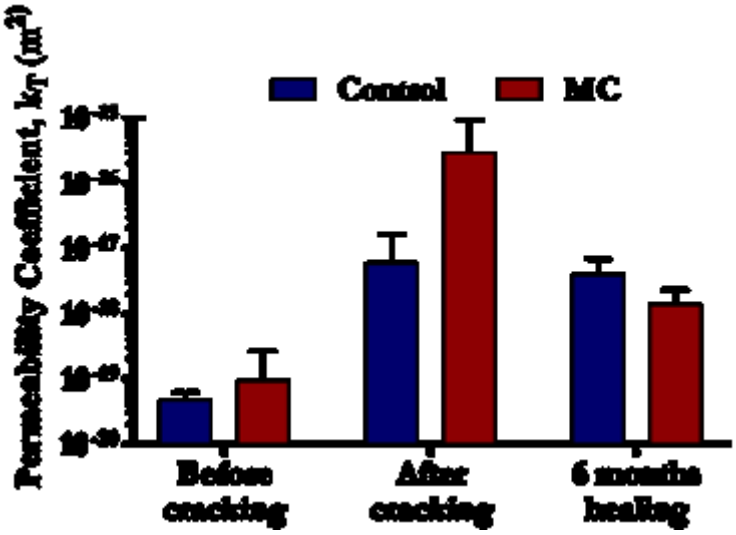

(a)

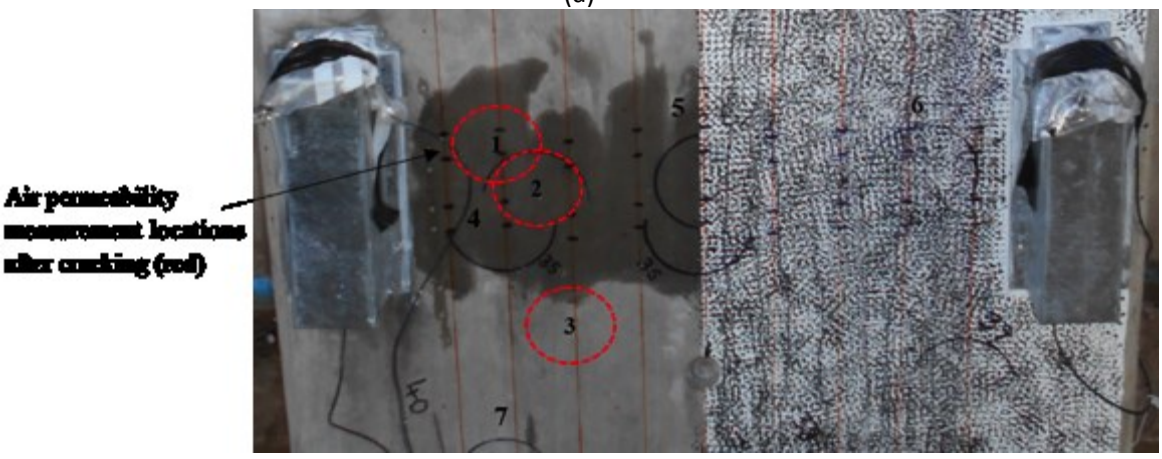

(b)

Figure 17 (a) Permeability of wall panels before cracking, after cracking and after a 6-month healing period and (b) Air permeability measurement locations after loading and subsequent cracking of concrete wall panel.

3.4 Microstructural analysis

Extracted cores were placed in a CT scanner and a typical image is shown in Figure 18. The figure and a detailed assessment of the CT scan images throughout the sample, confirmed uniform distribution of the microcapsules and their intact nature. The shell material was associated with a circular shaped low density material filled with a solid material, as shown in Fig. 18. The circular shape was typically ~250-350 µm, similar size to the microcapsules As the material is filled with a solid, and not air, we believe that the microcapsules have maintained their functionality yet the core material initially liquid, may have solidified in the time of investigation. Namely the osmotic difference has attracted gradually the water molecules outside of the shell wall to the surrounding matrix. Hence the solid/crystalline sodium silicate (the healing agent) is still within the microcapsules but not in its original liquid state.

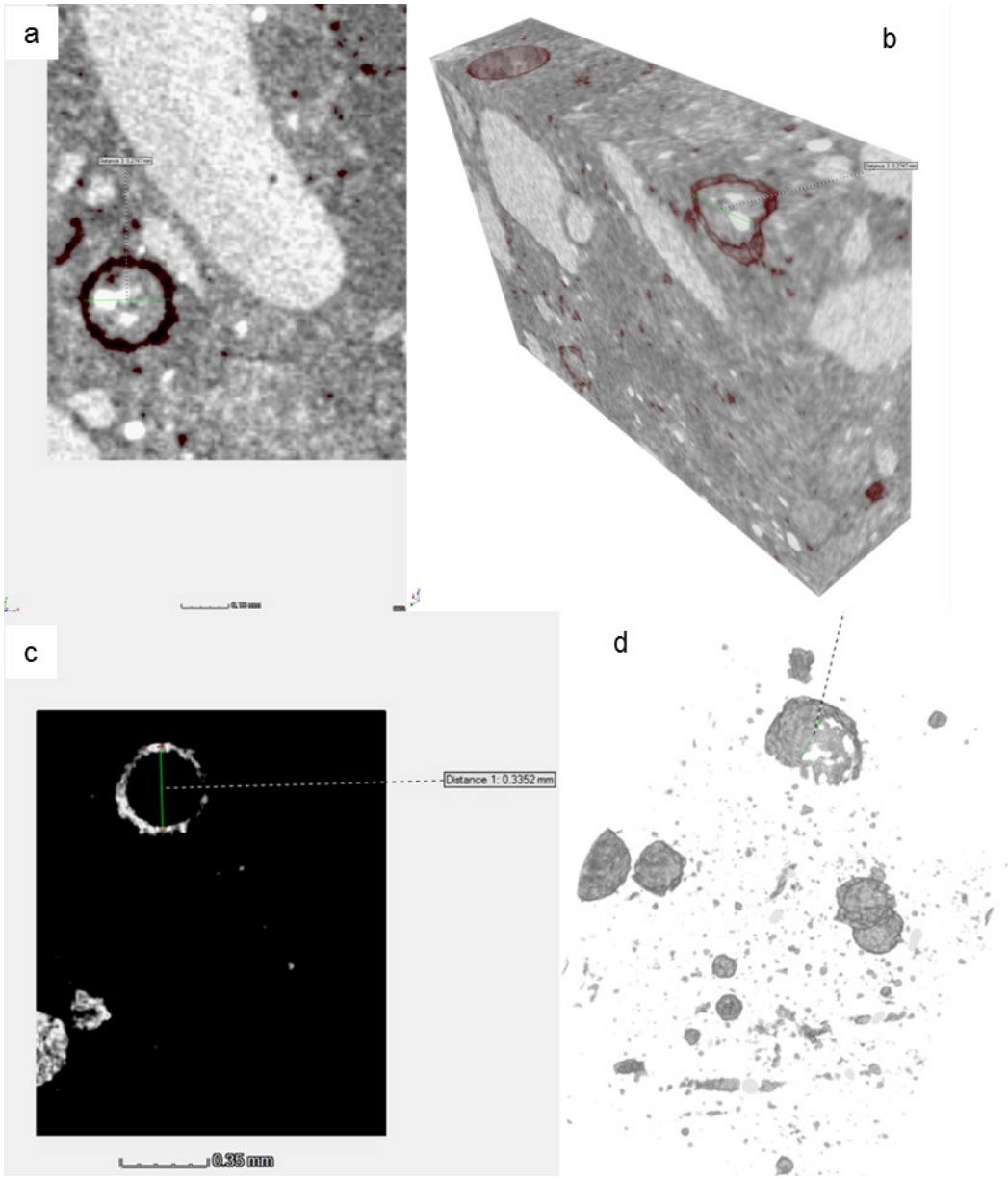

Figure 18 µCT scan image of a core from the microcapsule wall.

Extracted materials of the crack surface from both panels were observed using an SEM to characterise the healing products and typical images are presented in Fig. 19a-e. Fig. 19a shows multiple smooth cavities left by either debonded or ruptured microcapsules together with microcracks throughout the image attracted to, and passing through, the microcapsule locations. This is in agreement with previous observations whereby the presence of microcapsules were seen to provide a preferential path for cracks in mortar [21]. This phenomenon is considered beneficial for this self-healing system as it ensured microcapsules can be ruptured during crack propagation. Fig. 19b shows hexagonal calcium hydroxide crystals indicating their formation in the periphery of the microcapsules although on the crack surface, little, if any, can be seen. Instead, calcium carbonate and copious C-S-H flakes were observed. The former of these observations agree with previous findings that microcapsules act as nucleation sites for portlandite formation [43] whilst the latter of these products may be attributed to the reaction of the encapsulated sodium silicate with portlandite [39].

As the pieces of concrete material were extracted from near the crack mouth, the increased quantity of observed carbonation products is not surprising due to direct exposure to the external

environment and CO_2. SEM images also show products that have precipitated within small spherical voids of entrained air (Fib. 19b) suggesting that the products were generated following hardening of the concrete and most likely not produced during the initial cement hydration process. Ruptured microcapsules embedded on the crack surface could also be seen. In Fig. 19c, a crack approaching from the left-hand side is seen to pass through, or potentially debond, the microcapsule at this location. The stress concentration generated by the crack at this point was clearly not sufficient to rupture the microcapsule shell. However, on the right-hand side, the microcapsule shell is certainly ruptured and copious dense amorphous calcium silicate hydrate (C-S-H) phases are observed in the vicinity as suggested by the image brightness. In contrast, SEM images of samples extracted from the control panel (e.g. Fig. 19d and 19e) are consistently darker than those obtained from the microcapsule panel; indicating higher porosity in the matrix. The SEM images also show a variety of cement hydration products. Large calcium hydroxide crystals can be seen with other carbonation and C-S-H products on top. All of these SEM observations agree well with the expected autonomic self-healing mechanism whereby sodium silicate reacts with portlandite to produce C-S-H.

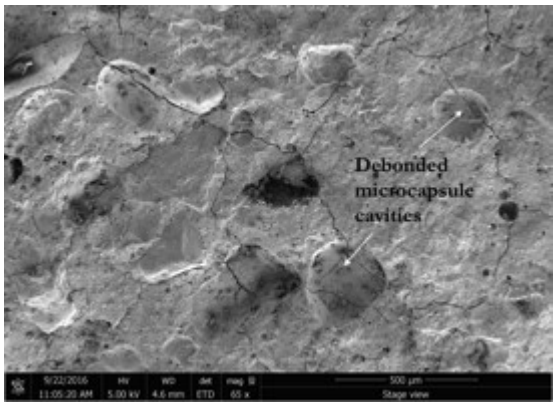

(a)

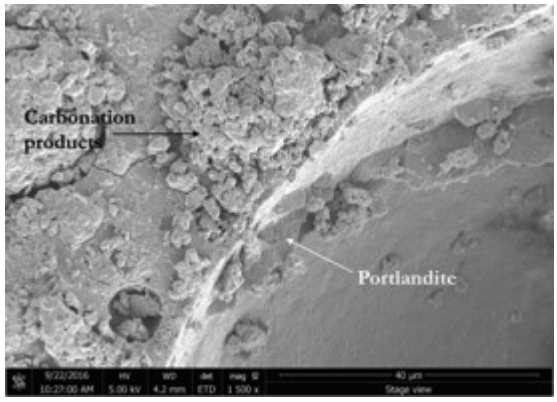

(b)

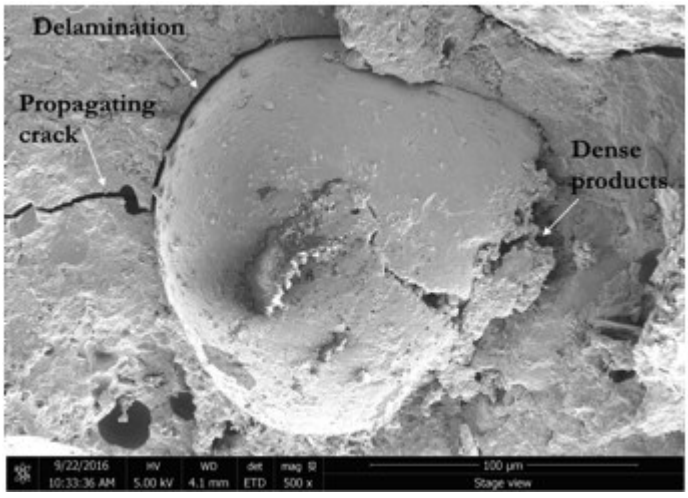

(c)

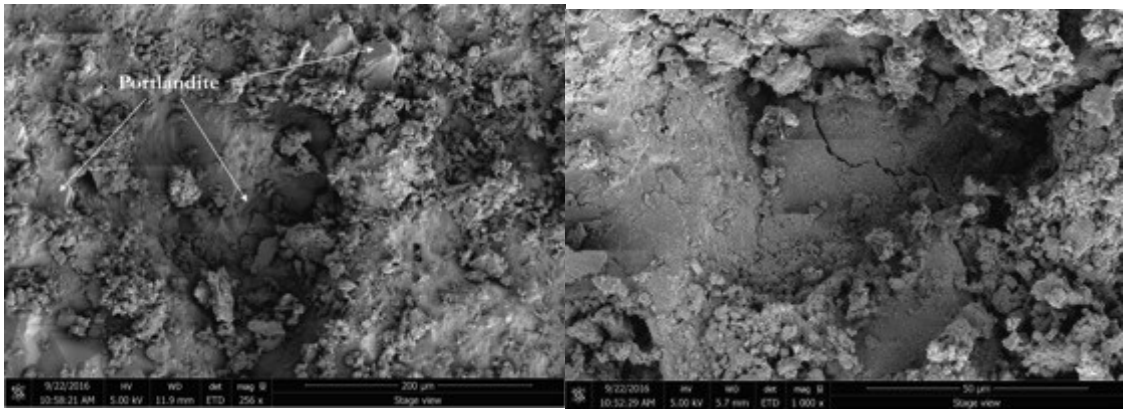

(d) (e)

Figure 19 Scanning electronic microscope (SEM) images from the MC and Control wall crack surfaces: (a) the attraction of microcracks towards microcapsule cavity locations; (b) crack surface adjacent to microcapsule cavity showing the deposition of carbonation and hydration products; (c) a ruptured microcapsule with dense hydration products at the outlet and (d, e) crack surface of the control wall showing high porosity and copious carbonation products.

XRD spectra for material extracted from both the microcapsule and control wall cracks after reloading revealed the same crystalline materials within the powdered samples, e.g. portlandite C-H, calcite and broad C-S-H peaks, with marginal differences observed (Fig. 20). This confirms that similar products have formed in the cracks. TGA/DTG tests (Fig. 21) showed similar quantities of portlandite and calcite with the portlandite content being quite very small. This is consistent with the SEM observations and is expected as portlandite close to the wall surface will carbonate to produce calcite. As mentioned previously, it has been observed that the portlandite content in cementitious samples increases when microcapsules are added into the mixture. Therefore, before damage occurs, an increased quantity of portlandite in expected to exist within the MC wall compared with the Control wall. However, when damage occurs and microcapsules are ruptured, sodium silicate is released and reacts with portlandite to produce C-S-H. Therefore, the portlandite content within a crack, and particularly in the vicinity of microcapsules, should reduce. As a result, the similar quantities of portlandite measured could actually indirectly suggest that the autonomic self-healing reactions did take place. The larger quantities of calcite measured in samples extracted from the microcapsule wall also support these observations. The larger quantities suggest that a greater proportion of portlandite existed previously in this region and ultimately in the microcapsule wall.

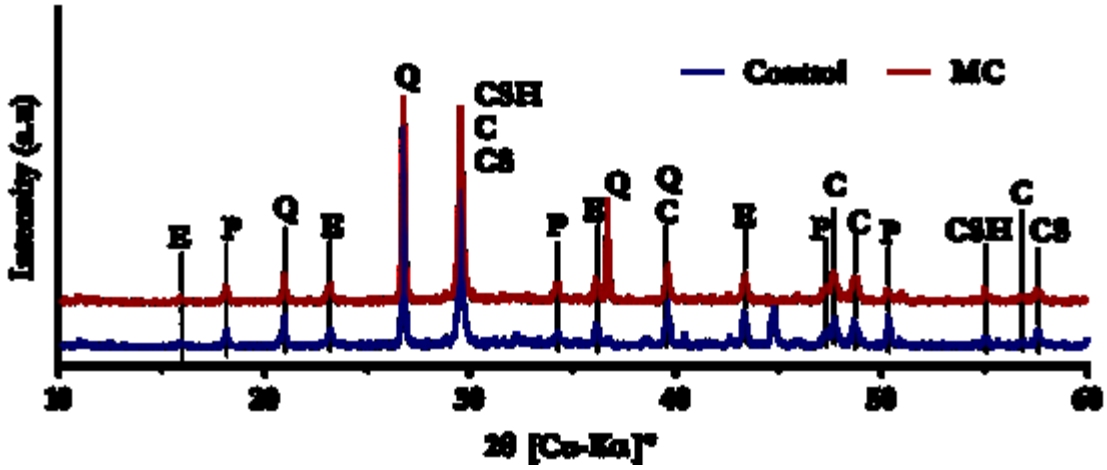

Figure 18 X-ray power diffraction (XRD) of powder extracted from MC and Control wall crack, where C: $CaCO_3$, CS: $2CaO{\cdot}SiO_2$, $3CaO{\cdot}SiO_2$, CSH: $3CaO{\cdot}2SiO_2{\cdot}4H_2O$, P: $Ca(OH)_2$ and Q: SiO_2.

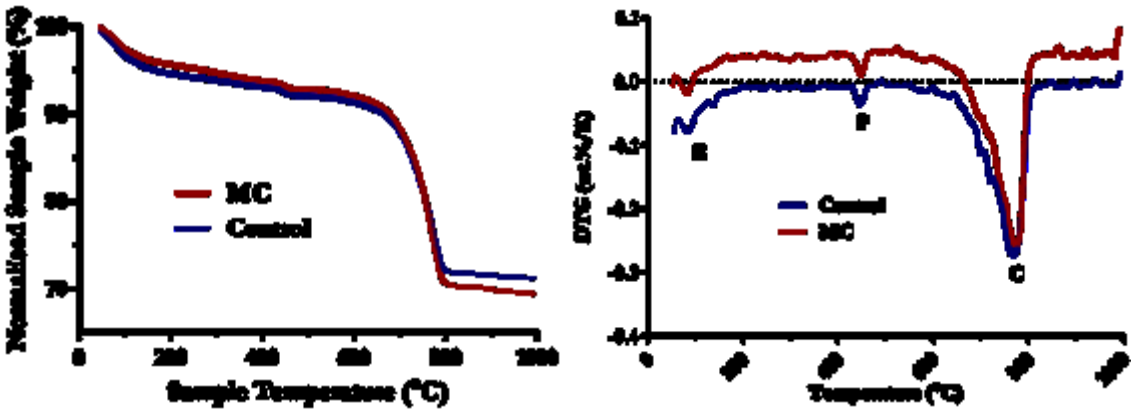

(a) (b)

Figure 19 Representative TGA/DTG graphs of powder extracted from crack faces of MC and control walls (a) TGA weight loss, (b) DTG curves where E: ettringite, P: portlandite and C: calcite

It is worth noting that it is difficult to distinguish between a reduction in portlandite due to reaction with the sodium silicate or carbonation to form calcite. However, these cumulative measurements support the hypothesis that a greater portlandite content existed in the microcapsule wall prior to cracking and has either been converted to calcite or reacted with the healing agent to form C-S-H. Furthermore, the increased quantity of calcite measured in the microcapsule wall sample is consistent with the increased visual healing that was observed at the crack mouth.

3.5 Healing mechanism

Coupling non-destructive testing results with macroscopic and microscopic observations it is possible to theorise the self-healing mechanism that had taken place in both walls. In both walls, the observed width at the crack mouth consistently reduced between monitoring events #1 and #4, mainly due to the precipitation of calcite. These monitoring events took place between November and February whereby air temperatures gradually decreased and daily rainfall increased. However, between monitoring events #4 and #5, less carbonates filled the crack mouth and the measured crack width increased. It is believed that the increased rainfall washed products that had precipitated at the crack mouth deeper into the crack and towards the crack tip (shown schematically in Fig. 22). The crack depth measurements taken at monitoring event #5 (Fig. 16)

support this. However, the reduction in crack depth was also caused by autogenic healing at the crack tip. At this location, healing was most likely to occur due to the close proximity of fracture surfaces. TGA of healing products on the crack surface and at the crack mouth revealed the large quantity of calcite present. In particular, a greater quantity of calcite was observed in the microcapsule wall crack. This is in agreement with the crack width observations in which the microcapsule wall saw greater areal healing. Since greater quantities of calcite precipitated at the crack mouth, a greater amount was washed into the crack. Therefore, greater healing at the crack mouth resulted in greater healing at the crack tip. However, these results also showed that healing at the crack mouth did not necessarily correspond to healing inside the crack.

The significant reduction in crack depth in the microcapsule wall hence cannot be due to the deposition of calcite alone. As well as the contribution from autogenic healing, autonomic healing due to the release of microencapsulated sodium silicate occurred. Microcapsules on the crack surface that were embedded within the cementitious matrix showed rupture and formed dense hydration products at the outlet. TGA results also showed a greater degree of hydration for the microcapsule wall; suggesting more hydration processes had occurred in comparison with the Control panel. Finally, air permeability measurements taken around the crack location also showed significant healing for the microcapsule wall in comparison to almost no healing in the Control wall (Fig. 17). These results are particularly useful as they provide insight into the densification of the bulk material due to self-healing processes taking place internally at other microcrack locations.

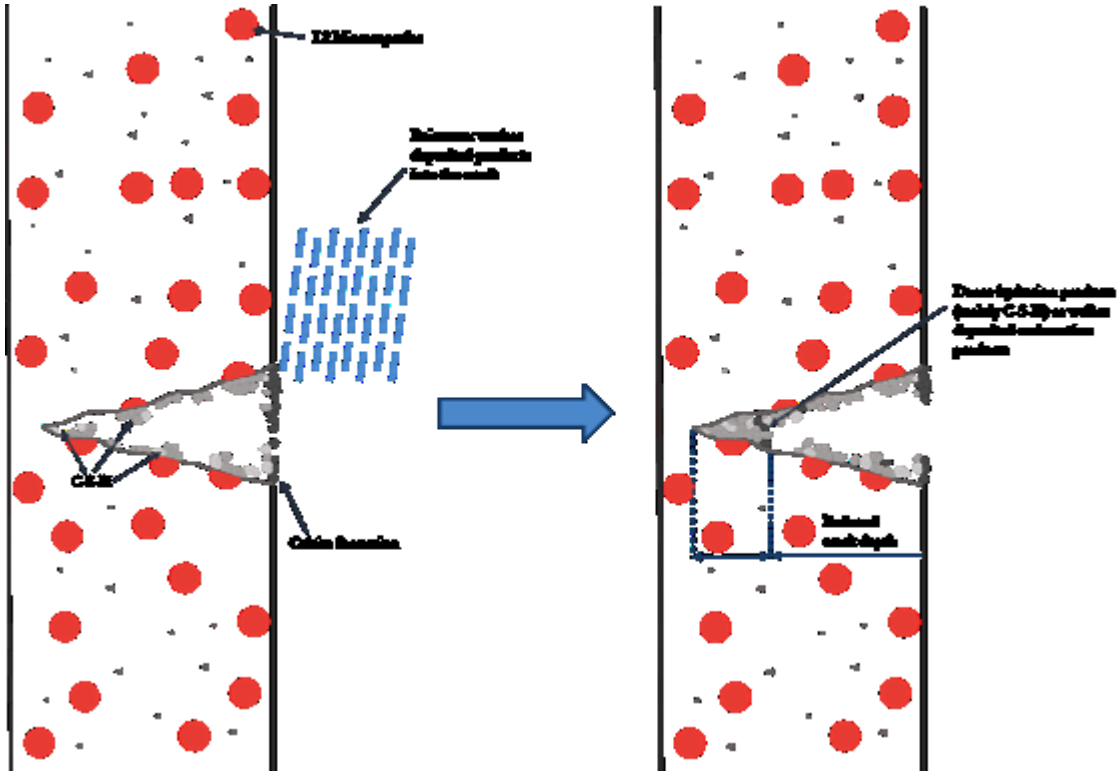

Figure 22 Healing mechanism of concrete wall panels: Carbonation products at the crack mouth are washed into the crack. This, along with autogenic and autonomic healing along the crack length and tip lead to a reduction in crack depth measurements.

4 Conclusions

The work presented here is part of the first major self-healing concrete site trial in the UK. It is the first successful attempt to scale up and implement self-healing concrete incorporating microcapsules on site. Self-healing concrete using microencapsulated sodium silicate was cast on-site in a retaining wall panel together with a control panel for comparison purposes. The walls were mechanically

cracked after 35 days of curing and then reloaded and monitored for self-healing over a 6-month period using air permeability, crack depth and microscopic crack width measurements. Although the addition of 8% microcapsules, by volume of the cement, was found to slightly reduce the mechanical strength, the microcapsule wall showed improved crack-width reduction, crack-depth reduction and recovery in permeability, confirming the real-time feasibility of microcapsule-based healing. In particular:

- Accelerated crack healing along the main crack of 49% and 63% was evident as early as 14 days and 28 days for the microcapsule wall compared to 14% and 36% respectively for the control.
- The average crack depth was also seen to reduce by ~8% and ~39% after 14 days in the control and microcapsule walls respectively reaching a final ~20% and ~58% at the end of the monitoring period.
- These results were further confirmed by significant permeability recovery (almost greater than 2.5 orders of magnitude) for the microcapsule wall.
- A strength recovery of 25% was achieved in the microcapsule wall, achieving a 10% improvement over the control panel.
- A temporal variation of the healing progression was identified in both panels influencing final observations. Macroscopic observations showed some crack opening for both walls following the initial reduction in crack width. Yet healing at the end of the monitoring period for the microcapsule panel remained significantly higher compared to the control panel.
- Microscopic imaging and microstructural investigations of extracted samples from the crack planes suggested a self-healing mechanism similar to what was observed in laboratory investigations.
- µCT confirmed the survivability and good distribution of microcapsules on site. SEM images revealed dense products formed around embedded ruptured microcapsules confirming the hypothesised release mechanism.
- TGA and XRD results of extracted material from the crack surfaces showed copious carbonation products in both cases and increased quantities of calcium silicate hydrate (C-S-H) in the microcapsule wall further supporting previous findings on the beneficial contribution of the microencapsulated sodium silicate to the autonomic self-healing progress.

Although the cast panels were not used in a structural application, this is a valuable step in gaining the confidence of civil engineering contractors, designers and consultants to adopt disruptive technologies working towards reducing and removing the requirement for inspection, maintenance and repair of concrete structures.

Conflict of Interest

None.

Acknowledgements

The authors would like to thank all of those involved with the EPSRC Materials for Life (M4L) project; in particular, Dr Robert Davies, Dr Martins Pilegis and Dr Oliver Teal for their contribution to the field trials. The financial support from the EPSRC for the Materials for Life (M4L) project (EP/K026631/1) and Resilient Materials for Life (RM4L) Programme Grant (EP/P02081X/1) is gratefully acknowledged. The financial support from the EPSRC in the form of PhD studentships to Petros Giannaros and Chrysoula Litina is also gratefully acknowledged.

References

[1] UK Treasury, National Infrastructure Delivery Plan 2016–2021, HM Treasury,

696 London, 2016. www.gov.uk/government/publications.
697 [2] ONS, Construction output in Great Britain: May 2016, (2016).
698 https://www.ons.gov.uk/.
699 [3] G. Tilly, J. Jacobs, Concrete repairs: Performance in service and current practice, BRE
700 Press, UK., 2007.
701 [4] World Economic Forum, The Boston Consulting Group, A Breakthrough in Mindset
702 and Technology - Shaping the Future of Construction, 2016.
703 [5] European Commission, Business Innovation Observatory - Smart Living: Advanced
704 Building Materials, 2014.
705 [6] Government Office For Science, Technology and Innovation Futures, 2017.
706 [7] i3P, Technology Roadmap for UK Construction & National Infrastructure, 2017.
707 https://www.i3p.org.uk/wp-content/uploads/2017/07/i3P-CI-Technology-Roadmap-Booklet-
708 FINAL.pdf.
709 [8] M. de Rooij, K. Van Tittelboom, N. De Belie, E. Schlangen, Self-Healing Phenomena in
710 Cement-Based Materials State-of-the-Art Report of RILEM Technical Committee 221-SHC:
711 Self-Healing Phenomena in Cement-Based Materials, RILEM 2013, 2013.
712 [9] N. De Belie, E. Gruyaert, A. Al-Tabbaa, P. Antonaci, C. Baera, D. Bajare, A.
713 Darquennes, R. Davies, L. Ferrara, T. Jefferson, C. Litina, B. Miljevic, A. Otlewska, J. Ranogajec,
714 M. Roig-Flores, K. Paine, P. Lukowski, P. Serna, J.-M. Tulliani, S. Vucetic, J. Wang, H.M.
715 Jonkers, A Review of Self-Healing Concrete for Damage Management of Structures, Adv.
716 Mater. Interfaces. (2018) 1800074. doi:10.1002/admi.201800074.
717 [10] L.L. Souza, A. Al-Tabbaa, Microfluidic fabrication of microcapsules tailored for self-
718 healing in cementitious materials, Constr. Build. Mater. 184 (2018) 713–722.
719 doi:10.1016/J.CONBUILDMAT.2018.07.005.
720 [11] B. Boh, Boštjan Šumiga, B. Šumiga, Microencapsulation technology and its
721 applications in building construction materials, RMZ - Mater. Geoenvironment. 55 (2008)
722 329–344.
723 [12] S.R. White, N.R. Sottos, P.H. Geubelle, J.S. Moore, M.R. Kessler, S.R. Sriram, E.N.
724 Brown, S. Viswanathan, Autonomic healing of polymer composites., Nature. 409 (2001) 794–
725 7. doi:10.1038/35057232.
726 [13] M. Pelletier, R. Brown, A. Shukla, A. Bose, Self-healing concrete with a
727 microencapsulated healing agent, Kingston, USA, 2011.
728 http://energetics.chm.uri.edu/system/files/ Self healing concrete -7-11.pdf.%0A[9].
729 [14] Z. Yang, J. Hollar, X. He, X. Shi, A self-healing cementitious composite using oil
730 core/silica gel shell microcapsules, Cem. Concr. Compos. 33 (2011) 506–512.
731 doi:10.1016/j.cemconcomp.2011.01.010.
732 [15] L. Ferrara, T. Van Mullem, M.C. Alonso, P. Antonaci, R.P. Borg, E. Cuenca, A.
733 Jefferson, P.-L. Ng, A. Peled, M. Roig-Flores, M. Sanchez, C. Schroefl, P. Serna, D. Snoeck, J.M.
734 Tulliani, N. De Belie, Experimental characterization of the self-healing capacity of cement
735 based materials and its effects on the material performance: A state of the art report by COST
736 Action SARCOS WG2, Constr. Build. Mater. 167 (2018) 115–142.
737 doi:10.1016/j.conbuildmat.2018.01.143.
738 [16] A. Kanellopoulos, T.S. Qureshi, A. Al-Tabbaa, Glass encapsulated minerals for self-
739 healing in cement based composites, Constr. Build. Mater. 98 (2015) 780–791.
740 doi:10.1016/j.conbuildmat.2015.08.127.
741 [17] T.S. Qureshi, A. Kanellopoulos, A. Al-Tabbaa, Encapsulation of expansive powder
742 minerals within a concentric glass capsule system for self-healing concrete, Constr. Build.
743 Mater. 121 (2016) 629–643. doi:10.1016/J.CONBUILDMAT.2016.06.030.
744 [18] C. Litina, A. Kanellopoulos, A. Al-Tabbaa, Alternative repair system for concrete using
745 microencapsulated healing agents, in: M. Grantham, M. Basheer, B. Magee, M. Soutsos
746 (Eds.), Proc. Concr. Solut. 5th Int. Conf. Concr. Repair, Taylor & Francis Group, Belfast, 2014:

747 pp. 97–103.
748 [19] A. Kanellopoulos, P. Giannaros, D. Palmer, A. Kerr, A. Al-Tabbaa, Polymeric
749 microcapsules with switchable mechanical properties for self-healing concrete: synthesis,
750 characterisation and proof of concept, Smart Mater. Struct. 26 (2017) 045025.
751 doi:10.1088/1361-665X/aa516c.
752 [20] P. Giannaros, A. Kanellopoulos, A. Al-Tabbaa, Sealing of cracks in cement using
753 microencapsulated sodium silicate, Smart Mater. Struct. 25 (2016) 084005.
754 doi:10.1088/0964-1726/25/8/084005.
755 [21] A. Kanellopoulos, P. Giannaros, A. Al-Tabbaa, The effect of varying volume fraction
756 of microcapsules on fresh, mechanical and self-healing properties of mortars, Constr. Build.
757 Mater. 122 (2016) 577–593. doi:10.1016/j.conbuildmat.2016.06.119.
758 [22] C.M. Dry, Repair and prevention of damage due to transverse shrinkage cracks in
759 bridge decks, 1999 Symp. Smart Struct. Mater. 3671 (1999) 253–256.
760 [23] T.D.P. Thao, Quasi-brittle self-healing materials: numerical modelling and
761 applications in civil engineering, PhD Thesis National Unviersity of Singapore, 2011.
762 [24] G. Karaiskos, E. Tsangouri, D.G. Aggelis, K. Van Tittelboom, N. De Belie, D. Van
763 Hemelrijck, Performance monitoring of large-scale autonomously healed concrete beams
764 under four-point bending through multiple non-destructive testing methods, Smart Mater.
765 Struct. 25 (2016). doi:10.1088/0964-1726/25/5/055003.
766 [25] C. Dry, IN-SERVICE REPAIR OF HIGHWAY BRIDGES AND PAVEMENTS BY INTERNAL
767 TIME-RELEASE REPAIR CHEMICALS, NCHRP-IDEA Progr. Proj. Final Rep. (2001).
768 https://trid.trb.org/view.aspx?id=692570 (accessed October 24, 2017).
769 [26] C.M. Dry, Self-repair of cracks in brittle material systems, in: SPIE 9800, Behav.
770 Mech. Multifunct. Mater. Compos. 2016, Las Vegas, 2016. doi:10.1117/12.2218564.
771 [27] H.M. Jonkers, E. Schlangen, Self-healing of cracked concrete: A bacterial approach,
772 6th Int. Conf. Fract. Mech. Concr. Concr. Struct. 3 (2007) 1821–1826.
773 [28] E. Tziviloglou, V. Wiktor, H.M. Jonkers, E. Schlangen, Bacteria-based self-healing
774 concrete to increase liquid tightness of cracks, Constr. Build. Mater. 122 (2016) 118–125.
775 doi:10.1016/j.conbuildmat.2016.06.080.
776 [29] M.G. Sierra-Beltran, H.M. Jonkers, M. Ortiz, Field application of self--healing
777 concrete with natural fibres as linings for irrigation canals in Ecuador, Fifth Int. Conf. Self-
778 Healing Mater. (2015) 32.
779 [30] A. Stewart, The 'living concrete' that can heal itself, CNN. (2016).
780 https://edition.cnn.com/2015/05/14/tech/bioconcrete-delft-jonkers/index.html.
781 [31] K. Paine, R. Lark, A. Al-Tabbaa, Biomimetic multi-scale damage immunity for
782 concrete, in: UKIERI Concr. Congr. Concr. Res. Driv. Profit Sustain., Jalandhar (Punjab), India,
783 2015. http://opus.bath.ac.uk/48322/.
784 [32] R.J. Lark, A. Al-Tabbaa, K. Paine, Biomimetic multi-scale damage immunity for
785 construction materials : M4L Project overview, in: 4th Int. Conf. Self-Healing Mater., Ghent,
786 2013: pp. 2–5.
787 [33] A. Al-Tabbaa, B. Lark, K. Paine, T. Jefferson, C. Litina, D. Gardner, T. Embley,
788 Biomimetic Cementitious Construction Materials for Next Generation Infrastructure, Proc.
789 Inst. Civ. Eng. - Smart Infrastruct. Constr. (2018) 1–35. doi:10.1680/jsmic.18.00005.
790 [34] O. Teall, R. Davies, M. Pilegis, A. Kanellopoulos, T. Sharma, K. Paine, A. Jefferson, R.
791 Lark, D. Gardner, A. Al-Tabbaa, Self-healing concrete full-scale site trials, in: K. Maekawa, A.
792 Kasuga, J. Yamazaki (Eds.), Proc. 11th Fib Int. PhD Symp. Civ. Eng., Tokyo, Japan, 2016: pp.
793 639–646.
794 [35] R. Davies, O. Teall, M. Pilegis, A. Kanellopoulos, T. Sharma, A. Jefferson, D. Gardner,
795 A. Al-Tabbaa, K. Paine, R.J. Lark, Large Scale Application of Self-Healing Concrete: Design,
796 Construction and Testing, Front. Mater. 5 (2018) 51. doi:10.3389/FMATS.2018.00051.
797 [36] P. Giannaros, A. Kanellopoulos, A. Al-Tabbaa, Damage recovery in self-healing

concrete, in: Heal. Conf., Delft, The Netherlands, 2016.
[37] R.J. Torrent, A two-chamber vacuum cell for measuring the coefficient of permeability to air of the concrete cover on site, Mater. Struct. 25 (1992) 358–365. doi:10.1007/BF02472595.
[38] R. Alghamri, A. Kanellopoulos, A. Al-Tabbaa, Impregnation and encapsulation of lightweight aggregates for self-healing concrete, Constr. Build. Mater. 124 (2016) 910–921. doi:10.1016/j.conbuildmat.2016.07.143.
[39] S. Irico, A. Bovio, G. Paul, E. Boccaleri, D. Gastaldi, L. Marchese, L. Buzzi, F. Canonico, A solid-state NMR and X-ray powder diffraction investigation of the binding mechanism for self-healing cementitious materials design: The assessment of the reactivity of sodium silicate based systems, Cem. Concr. Compos. (2016). doi:10.1016/j.cemconcomp.2016.11.006.
[40] S. Jacobsen, J. Marchand, H. Hornain, Sem observations of the microstructure of frost deteriorated and self-healed concretes, Cem. Concr. Res. 25 (1995) 1781–1790. doi:10.1016/0008-8846(95)00174-3.
[41] C. Edvardsen, Water permeability and autogenous healing of cracks in concrete, ACI Mater. J. 96-M56 (1999) 448–454.
[42] L. Ebensperger, R. Torrent, Concrete air permeability “in situ” test: status quo, Rev. Ing. Construcción. 25 (2011) 371–382.
[43] M. Aguayo, S. Das, A. Maroli, N. Kabay, J.C.E. Mertens, S.D. Rajan, G. Sant, N. Chawla, N. Neithalath, The influence of microencapsulated phase change material (PCM) characteristics on the microstructure and strength of cementitious composites: Experiments and finite element simulations, Cem. Concr. Compos. 73 (2016) 29–41. doi:10.1016/j.cemconcomp.2016.06.018.